



Enhanced electrochemical performance of MnO₂/NiO nanocomposite for supercapacitor electrode with excellent cycling stability

K. Mohamed Racik^{1,2} · K. Guruprasad³ · M. Mahendiran^{1,2} · J. Madhavan¹ · T. Maiyalagan³ · M. Victor Antony Raj^{1,2}

Received: 14 November 2018 / Accepted: 25 January 2019 / Published online: 5 February 2019
© Springer Science+Business Media, LLC, part of Springer Nature 2019

Abstract

Transition metal oxides with metallic composites have greater attention for hybrid supercapacitor due to their excellent electrochemical performance and low cost. In this study, the preparation of manganese dioxide/nickel oxide (MnO₂/NiO) nanocomposite via a facile hydrothermal method is reported. The crystallographic and morphological features were studied by Powder XRD, FTIR, HRSEM, EDX and TEM analysis. Cyclic voltammetry, galvanostatic charge–discharge and impedance analysis are implemented in order to examine the applicability of the MnO₂/NiO nanocomposite electrode material as a supercapacitor. The MnO₂/NiO composites revealed good electrochemical performance by exhibiting a specific capacitance of 247 Fg⁻¹ at the discharge current density rate of 0.5 Ag⁻¹ using 1 M KOH as the electrolyte. Moreover, the composite electrode shows enhanced cycling stability. The improvement in specific capacitance of the MnO₂/NiO composite is primarily due to its hybrid structure, which offers a better contact of surface of electrode and electrolyte, and active sites with large scale. These results expose the development of MnO₂/NiO electrode material shown enhanced performance for supercapacitors.

1 Introduction

In this energy-dependent world, electrochemical devices for energy storage play a energetic role in overcoming the depleting fossil fuels [1]. Supercapacitors received impeccable interest in academic and industrial world in recent years owing to their fast charge/discharge rate, high power density and extensive cycling life [2–4]. Supercapacitors and batteries are similar arrangements with negative and positive electrodes and separators soaked in electrolytes [5, 6]. Supercapacitors are broadly categorized into two types, i.e., double layer electrical capacitors (EDLC) and pseudocapacitors [7]. In the case of EDLC, the capacitance comes from accumulation of charges on electrode–electrode interfaces. Furthermore, the storage of pseudocapacity energy is carried out by transferring the faradic charges between electrolyte

and electrode, due to reversible multielectronic redox phase reactions [8].

Among the electrode materials for pseudocapacitors, MnO₂ has been widely studied due to low cost, low toxicity, large theoretical capacity (~ 1370 Fg⁻¹) and natural abundance [9]. For enhancement in specific capacity of MnO₂, synthesis of nanostructured electrodes based on MnO₂ with new morphologies, porous hierarchical structures, high surface area and greater pore volume were explored using various methods [9–11]. MnO₂-based nanomaterials with granulometry, morphology, crystallinity, high specific surface area and good controllable electrical conductivity are critical to improving capacity, rate capability [12–14]. To improve MnO₂-based electrodes, fabrication of MnO₂-based compounds incorporating with porous metal substrates, conductive polymers, carbon and graphene etc. [15–17]. Nickel oxide (NiO) is widely studied as one of the most promising pseudocapacitive materials possessing an unusually high specific theoretical capacity (2573 Fg⁻¹) [18] and an excellent reactivity of electrochemical reaction. The morphologically controlled preparation of NiO has a great influence on its performance [19].

In recent times, much attention has been engrossed to improve the specific capacitance of the supercapacitors, exploring new materials with the rational intention of the multi-component combination [20, 21], which provides

✉ M. Victor Antony Raj
vicvad2003@yahoo.co.in

¹ Department of Physics, Loyola College, Chennai, India

² Loyola Institute of Frontier Energy (LIFE), Loyola College, Chennai, India

³ Department of Chemistry, SRM Institute of Science and Technology, Kattankulathur, Chennai 603203, India

synergistic effect of all the individual component, as well as the control 3D hierarchical heterostructures, which maintain a large external surface and provide effectual and fast routes for the transport of ions and electrons, thus high capacitance at fast charging–discharging rates. Although the individual capacitive properties of NiO and MnO₂ have been widely demonstrated [22–24], the electrochemical capacity of the compounds has also received some interest and is expected to be a desirable material for the high performance supercapacitor. For example, Liu et al. reported the fabrication of NiO/MnO₂ hybrid nanostructures in the stainless steel substrate by interfacial reactions to pseudocapacitors, which have a high area capacity of 0.35 F cm⁻² [25]. Li et al. established fabrication of hierarchical matrices of NiO/MnO₂ nanosheets on carbon fiber paper through the hydrothermal process, which could provide a real specific capacity of 1.0 F cm⁻² (494.8 F g⁻¹) [26]. Junjiao Chen et al. fabricated NiO@MnO₂ core/shell nanocomposites by a two-step method which exhibited a specific capacitance of 266.7 F g⁻¹ at 0.5 A g⁻¹ and excellent cycling stability (81.7% retention after 2000 cycles at 1 A g⁻¹) [27]. Bi et al. reported microwave synthesis of NiO/MnO₂ composite which revealed a specific capacitance of 102.78 mAh g⁻¹ at 1 A g⁻¹ and superior cycling stability with specific capacitance retention of 140% over more than 1500 cycles [28]. Xi et al. synthesized NiO/MnO₂ core–shell nanoflakes on carbon cloth with areal capacitance of 316.37 mF cm⁻² and special gravimetric capacitance of 204.3 F g⁻¹ at the scan rate of 50 mV s⁻¹. The electrode retains 89% of its initial discharge capacitance after 2200 cycles with >97% Coulombic efficiency [29]. However, the synthetic procedures for these NiO/MnO₂ core–shell structures are relatively complicated. Therefore, a simple wet chemical approach to prepare MnO₂/NiO nanocomposite is essential.

In this study, we have reported facile hydrothermal route for the preparation of manganese dioxide/nickel oxide (MnO₂/NiO) nanocomposite. The structure and optical morphology of bare MnO₂, NiO and MnO₂/NiO nanocomposite were examined by XRD, HRSEM, TEM, and FT-IR techniques. The electrochemical features were inspected by CV, GCD and EIS techniques. The results emphasize that the MnO₂/NiO nanocomposites are capable electrode materials for supercapacitors.

2 Experimental

2.1 Preparation of MnO₂ nanoparticles

The MnO₂ nanoparticles were synthesized by a simple and economical hydrothermal method. Typically, MnCl₂·4H₂O and urea were dissolved in 50 ml of deionized water to form a homogeneous solution. Then, the above solution was

transferred into Teflon autoclave and set aside at 120 °C for 24 h. The resulting nanoparticles and nanocomposite powders were washed three times with 100 ml of DI water and three times in ethanol. Finally, the powder was dried at 80 °C for 12 h. Finally, the sample was obtained by sintering the precipitate at 400 °C for 3 h.

2.2 Preparation of NiO nanoparticles

For the synthesis of NiO nanoparticles, 3.239 g NiCl₂·6H₂O was dissolved in 50 ml distilled water. Then, 1.502 g urea was added into the obtained nickel chloride solution under dynamic stirring for 30 min (nickel chloride to urea ratio = 1:1). Then the mixed solution was transferred into a Teflon-lined autoclave (100 ml), sealed and kept at 120 °C for 24 h. Centrifugation is employed to separate the precipitate of the mixed solution with deionized water and ethanol. Finally, the powder was dried at 80 °C for 24 h. Resultant NiO nanopowder was obtained by sintering the precipitate at 400 °C for 2 h.

2.3 Preparation of MnO₂/NiO nanocomposite

For the MnO₂/NiO nanocomposite preparation, the above synthesized NiO was dissolved in 20 ml distilled water by magnetic stirring, then MnCl₂·4H₂O and urea was mixed into the dispersion. After continuously stirring for 1 h, the mixed solution was moved into a 150 ml autoclave at 120 °C for 24 h. The black colour precipitate obtained from above process was collected by filtration and washing with deionized water and ethanol. The resulting final product was dried at 80 °C for 12 h and sintered at 400 °C for 4 h.

2.4 Characterizations

The XRD patterns were recorded in a Rigaku D/max-kA diffractometer with Cu K α radiation. The morphologies were observed by scanning electron microscopy (HRSEM, FEI Quanta FEG 200), and the TEM images were obtained on a Philips CM200FEG field emission microscope. Energy dispersive X-ray spectroscopy (EDX, FEI Quanta FEG 200), and FTIR spectroscopy (Perkin Elmer) measurements were used to investigate the prepared composites.

2.5 Electrochemical measurements

Electrochemical properties of bare MnO₂, NiO and MnO₂/NiO nanocomposite were inspected by cyclic voltammetry (CV), galvanostatic charge and discharge (GCD) and electrochemical impedance spectroscopy (EIS). Working electrode was made of active material (80% by weight), activated carbon (10% by weight) and polyvinylidene fluoride suspension (PVDF) (10% by weight) ratio using *N*-methyl-2-pyrrolidone

(NMP) as a solvent to make homogeneous slurry. After the slurry was pasted onto the nickel sheet current collector and dried at 80 °C for 24 h. All measurements were taken using an aqueous 1 M KOH as electrolyte at ambient conditions with the electrode material prepared as a working electrode, a platinum wire as a counter electrode and Ag/AgCl as a reference electrode.

3 Results and discussions

3.1 Powder XRD analysis

Figure 1 illustrates the XRD patterns of MnO₂, NiO and MnO₂/NiO nanocomposite. The prominent peaks appear at 2θ of 28.6°, 37.4°, 42.8°, 56.7°, 59.3°, and 72.4° can be indexed to be (110), (101), (111), (211), (220) and (301) crystal planes of tetragonal MnO₂ (JSPDS card no. 81-2261) [30]. For NiO, the peaks appear at 2θ of 37.2°, 43.1°, 62.9°, 75.4°, 79.4° resultant to the diffractions from (111), (200), (220), (311) and (222) of cubic NiO (JSPDS card no. 71-1179) [31]. No further peaks were detected, specifying the high degree of phase purity of NiO prepared in this work. The XRD pattern confirmed the cubic structure and lattice constant was calculated as a = b = c = 4.177 Å.

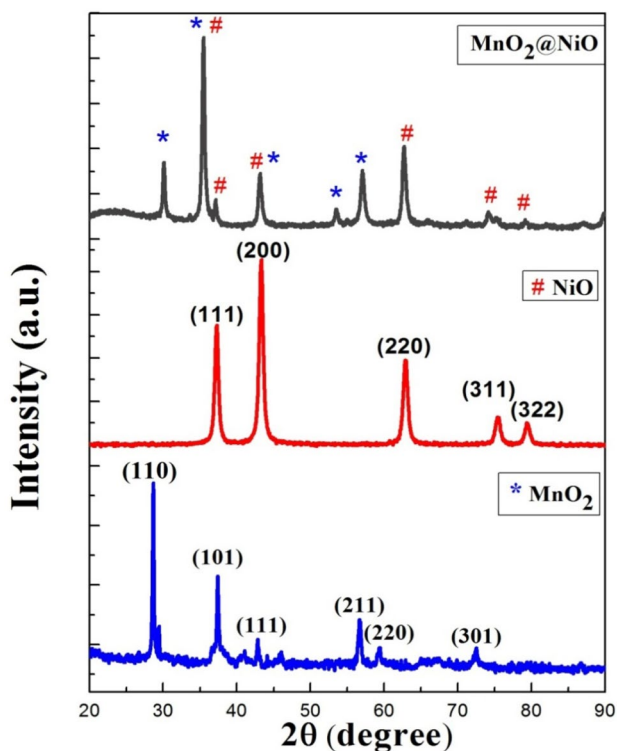


Fig. 1 XRD patterns of MnO₂ (blue line), NiO (red line) and MnO₂/NiO nanocomposite (black line)

XRD result confirms the successful preparation of MnO₂/NiO composites. The average crystallite size of NiO and MnO₂ is calculated to be 29.75 nm, 15.77 nm respectively. All the diffraction peaks of MnO₂/NiO nanocomposite are established to the NiO with cubic phase and other peaks are corresponding due to MnO₂. Furthermore, XRD does not detect any signals from other materials, which indicates the high purity of the synthesized product. Besides, the peak located at 37.3° became broad and shifted to a lower degree direction, which may be due to the overlap of (111) plane of NiO and (101) plane of MnO₂. The XRD results point out the coexistence of NiO and MnO₂.

3.2 FTIR analysis

The vibrational atom modes of MnO₂, NiO and MnO₂/NiO nanocomposites were confirmed by FTIR analysis as shown in Fig. 2. From MnO₂ spectra, the wide band around 3432 cm⁻¹ is ascribed to O–H stretching vibrations, indicating the hydrates nature of MnO₂. The absorption bands around 1627 and 1036 cm⁻¹ are assigned to bending vibrations of O–H combined with the Mn atoms. The peaks located around 538 and 434 cm⁻¹ are ascribed to Mn–O vibrations. From NiO, a large absorption band about 1637 cm⁻¹ is attributable to flexible vibration of H₂O

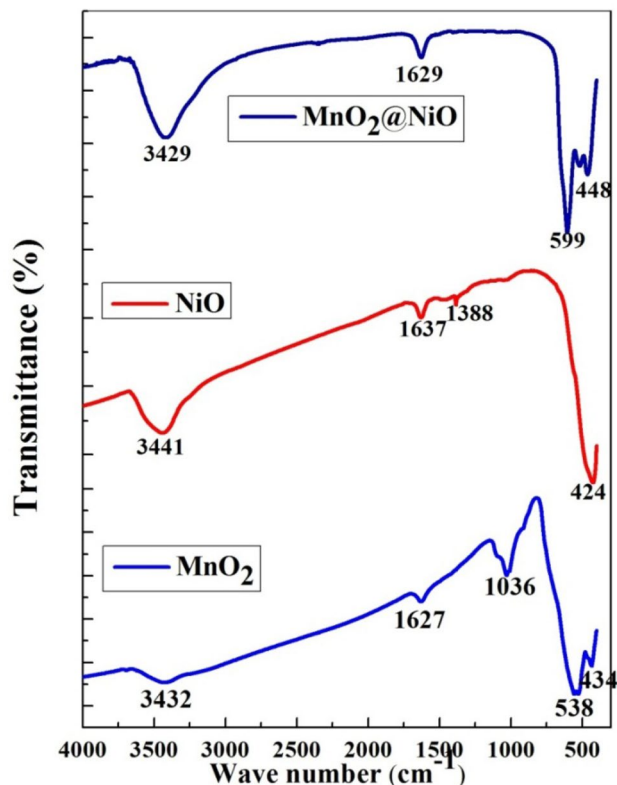


Fig. 2 FTIR spectrum of MnO₂, NiO and MnO₂/NiO nanocomposite

molecules. The band around 1388 cm^{-1} is due to presence of CO_3^{2-} anions. The 424 cm^{-1} strong band corresponds to the vibration of the Ni–O bond. As can be seen, the formation of MnO_2/NiO nanocomposite is confirmed with two strong bands at 448 and 599 cm^{-1} . These bands indicated the division of the vibratory band corresponding to the Ni–O or O–Mn–O bond [32]. The peak at 3429 cm^{-1} is due to stretching vibrations of the O–H adsorbed nanocomposite surfaces NiO and MnO_2/NiO . The peaks around 1629 cm^{-1} are shown with the vibration of chelators with symmetric and asymmetric COO^- formats.

3.3 Morphological studies

Figure 3 displays the HRSEM images of MnO_2 , NiO and MnO_2/NiO nanocomposite and confirmed that all the synthesized samples having the size is non-uniform. Hence it

may be the outcome of the combination of the spherical-shaped particles and the growth of non-equal crystalline grains during the preparation period. Due to low dosage of urea to precursor ratio of 1:1, the number of urea around Ni and Mn was very limited in the solution. In the course of the reaction, as the small amount of urea could not provide sufficient hydroxyl groups, therefore non-uniformly sized spherical like particles was formed, and the shape varied from spherical to rod like morphology after the reaction was carried out for 24 h. Similar results were found earlier for $\text{CeO}_2\text{--ZrO}_2$ nanocomposites [33]. From the HRSEM images, we concluded that the formation of spherical nanoparticles like structure, due to aggregation followed by the agglomeration of nanoparticles. It was illustrious that the particles are collected together, due to magnetic interaction between the particles [34, 35].

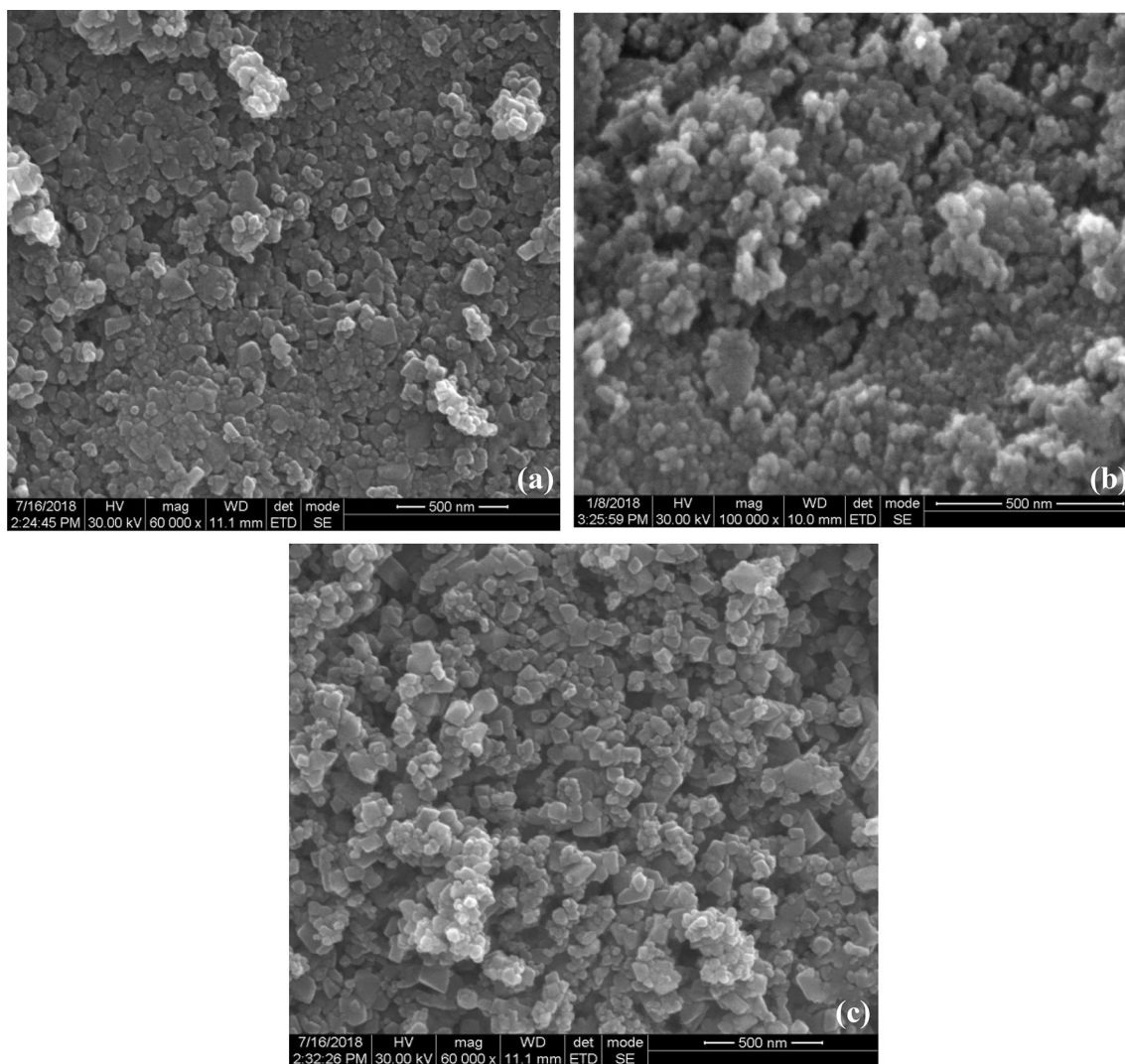


Fig. 3 HRSEM images for **a** MnO_2 , **b** NiO and **c** MnO_2/NiO nanocomposite

The elemental composition of electrode material is necessary for the supercapacitor energy storage application; for that reason, elemental and chemical compositions of MnO_2 , NiO and MnO_2/NiO nanocomposite were tested by EDX analysis. The EDX spectra of prepared samples were analyzed in binding region of 0–10 keV, which is shown in Fig. 4. Figure 4a and b reveal the presence of stoichiometric proportion of O, Mn and O, Ni in MnO_2 and NiO samples respectively, and Fig. 4c evidently confirms the presence of Mn, Ni, and O in MnO_2/NiO nanocomposite. The observed molar ratio is confirming the formation of MnO_2 , NiO and MnO_2/NiO nanocomposites (Fig. 4a–c inset).

The morphology and structural features of MnO_2 , NiO and MnO_2/NiO nanocomposite were described by HR-TEM analysis. The characteristic HR-TEM images are exposed in Fig. 5a–c. HR-TEM images show the nano-spherical structure with a diameter of 10–50 nm. The observed spherical shaped samples are formed by the small aggregation of nanoparticles, due to the magnetic natural surroundings of the materials. The SAED pattern of pristine MnO_2 , NiO and

MnO_2/NiO nanocomposite were shown in Fig. 6a–c confirmed the samples were well crystallized in nature.

3.4 Electrochemical measurements

The electrochemical performance of the prepared materials was studied through CV, GCD and EIS in 1 M aqueous KOH electrolyte without any binding or carbon additive. The CV measurements were made in a three-electrode arrangement with the reference electrode (Ag/AgCl) and a counter electrode (platinum foil). The CV measurement of the electrode was taken in potential range of –0.1 to 0.4 V. The two regions in CV plot indicate the area of negative current reduction at the cathode and positive current region of anode oxidation.

The CV graphical plots of NiO, MnO_2 and MnO_2/NiO composites are showed in Figure 7. Bare MnO_2 CV curve appears as rectangular shape without obvious redox peaks; capacitive behavior of MnO_2 nano spheres electrode is pseudocapacitance, attributed to the reversible redox reaction among Mn^{3+} and Mn^{4+} . It was attributed to cation

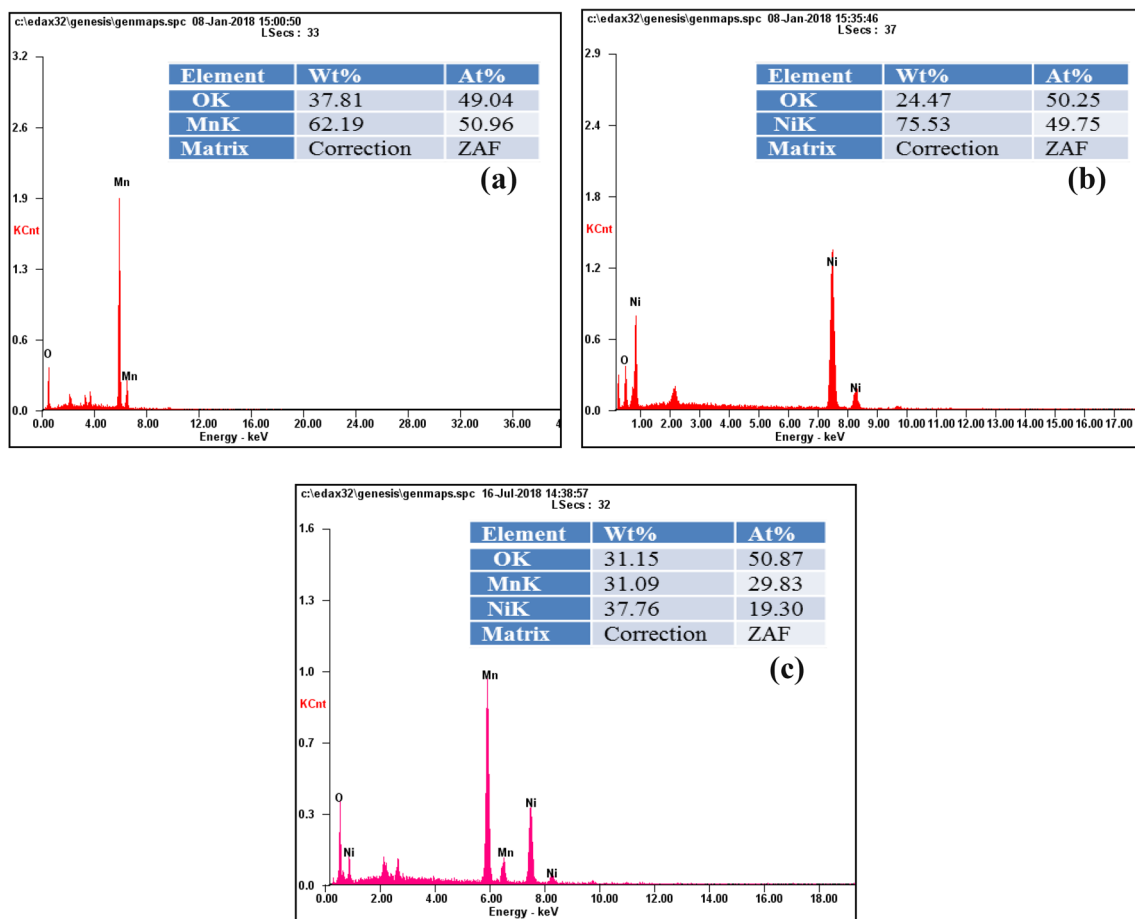


Fig. 4 EDX spectrum of a MnO_2 , b NiO and c MnO_2/NiO nanocomposite

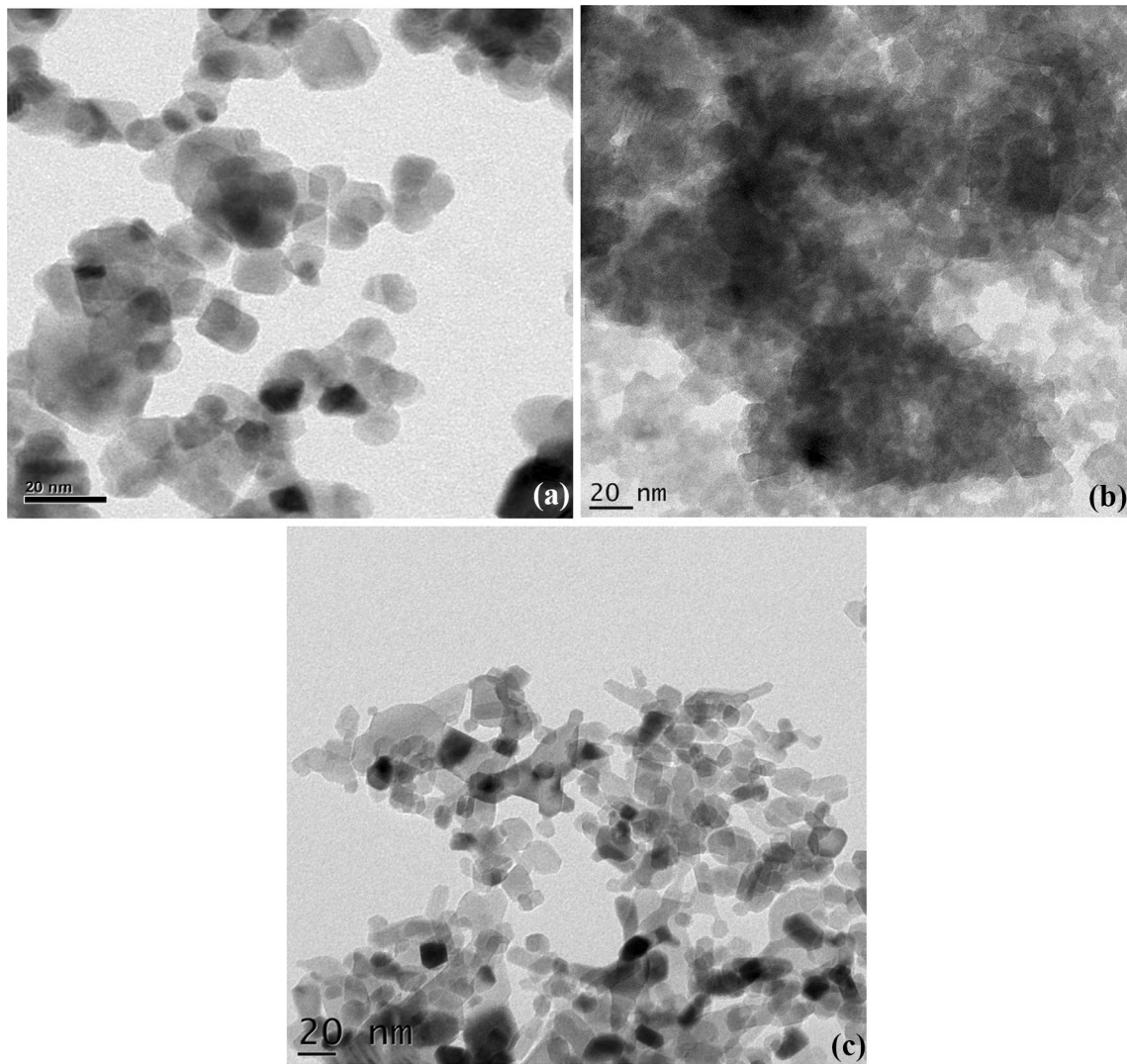


Fig. 5 TEM images of **a** MnO₂, **b** NiO and **c** MnO₂/NiO nanocomposite

surface adsorption (Ni⁺) of electrolyte and possible intercalation/deintercalation of Ni⁺ [36]. With the addition of NiO in MnO₂, the CV hybrid matrix shows a clear difference. The shape of the plot is not perfectly rectangular, which point out a deviation from ideal behavior of the supercapacitor. The plot contains some redox peaks which is observed in all CV curves. It suggests the pseudocapacitive characteristic of active materials, which is obviously different from the double layer electrical capacity characterized by almost rectangular CV curves, redox pairs correspond to reversible reactions of Ni²⁺/Ni³⁺ transitions [37]. The slight change in shape of the CV curves specifies the good charging rate capability of the electrode.

The galvanostatic charge–discharge (GCD) test was performed at a current density of 1 Ag⁻¹. The voltage range was maintained from -0.1 to 0.4 V during the GCD test,

as given in Fig. 8. The specific capacitance from the GCD plot can be calculated by the equation:

$$\text{Specific capacitance} = C_{\text{GCD}} = i \times \Delta t / (\Delta v \times m) \quad (1)$$

where i/m is the current density (Ag⁻¹), Δt corresponds to discharge time and Δv stand for potential range. The nature of the GCD plot deviates from ideal triangular pattern indicating that MnO₂/NiO composite material is pseudocapacitive in nature, which also supports the CV result. As given in Fig. 9, contrasting with specific capacitances of MnO₂ and NiO and MnO₂/NiO electrodes at various charge/discharge current, the capacitance of MnO₂/NiO reduces from 247.78 F g⁻¹ (current density of 0.5 A g⁻¹) to 56.21 F g⁻¹ (4 Ag⁻¹) with 22% of the specific capacitance remaining, in the same process, the capacitance of MnO₂ electrode reduces from 175.51 F g⁻¹ (0.5 A g⁻¹) to 37.47 F g⁻¹ (4 Ag⁻¹) with

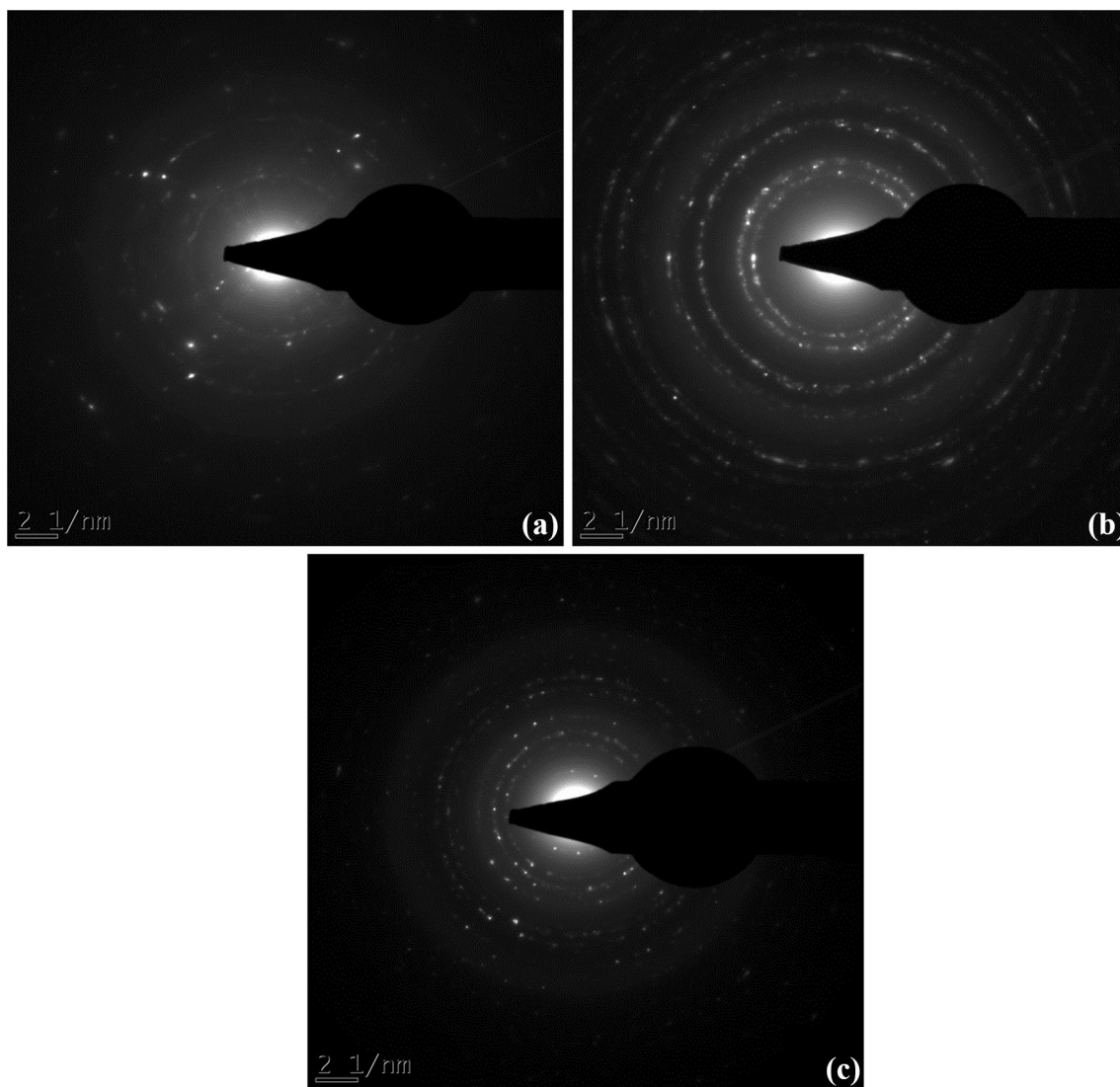


Fig. 6 SAED Pattern of **a** MnO₂, **b** NiO and **c** MnO₂/NiO nanocomposite

21% of the specific capacitance remaining, and the capacitance of NiO electrode reduces from 129.65 F g⁻¹ (0.5 Ag⁻¹) to 23.72 F g⁻¹ (4 Ag⁻¹) with 17% of the specific capacitance remaining. This result points out the specific capacitance of MnO₂/NiO electrode is much greater than pristine NiO and MnO₂ electrode nanoparticles. The higher specific capacitance of MnO₂/NiO electrode is due to NiO spherical nanoparticles were well wrapped on the surface of MnO₂ nanoparticles to provide composites with larger surface area. Our material also showed a better specific capacitance than the specific capacitance of MnO₂ electrode based composites. The energy density (E_d) values of the prepared electrode materials and power density (P_d) values were calibrated by following relations.

$$E_d = 0.5C_s \Delta V^2 \quad (2)$$

$$P_d = 3.6 \times \frac{E_d}{t} \quad (3)$$

where E_d is energy density (Wh kg⁻¹), C_s is specific capacitance (F g⁻¹), ΔV is potential window of discharge (V), P_d is power density (W kg⁻¹) and Δt is discharge time (s). The energy density is found to increase with the power density. The power density is in increasing trend which point out the pseudocapacitor discharging capacity is directly proportional to discharge current. At a current density of 4 Ag⁻¹, the MnO₂/NiO nanocomposites provided a higher energy density of 123.12 Wh kg⁻¹ and power density of 12.84 kW kg⁻¹. Table 1 exhibits the specific capacitance, energy and power density values of MnO₂, NiO and MnO₂/NiO nanocomposites. Table 2 presents the supercapacitor performance comparisons of MnO₂/NiO nanocomposites

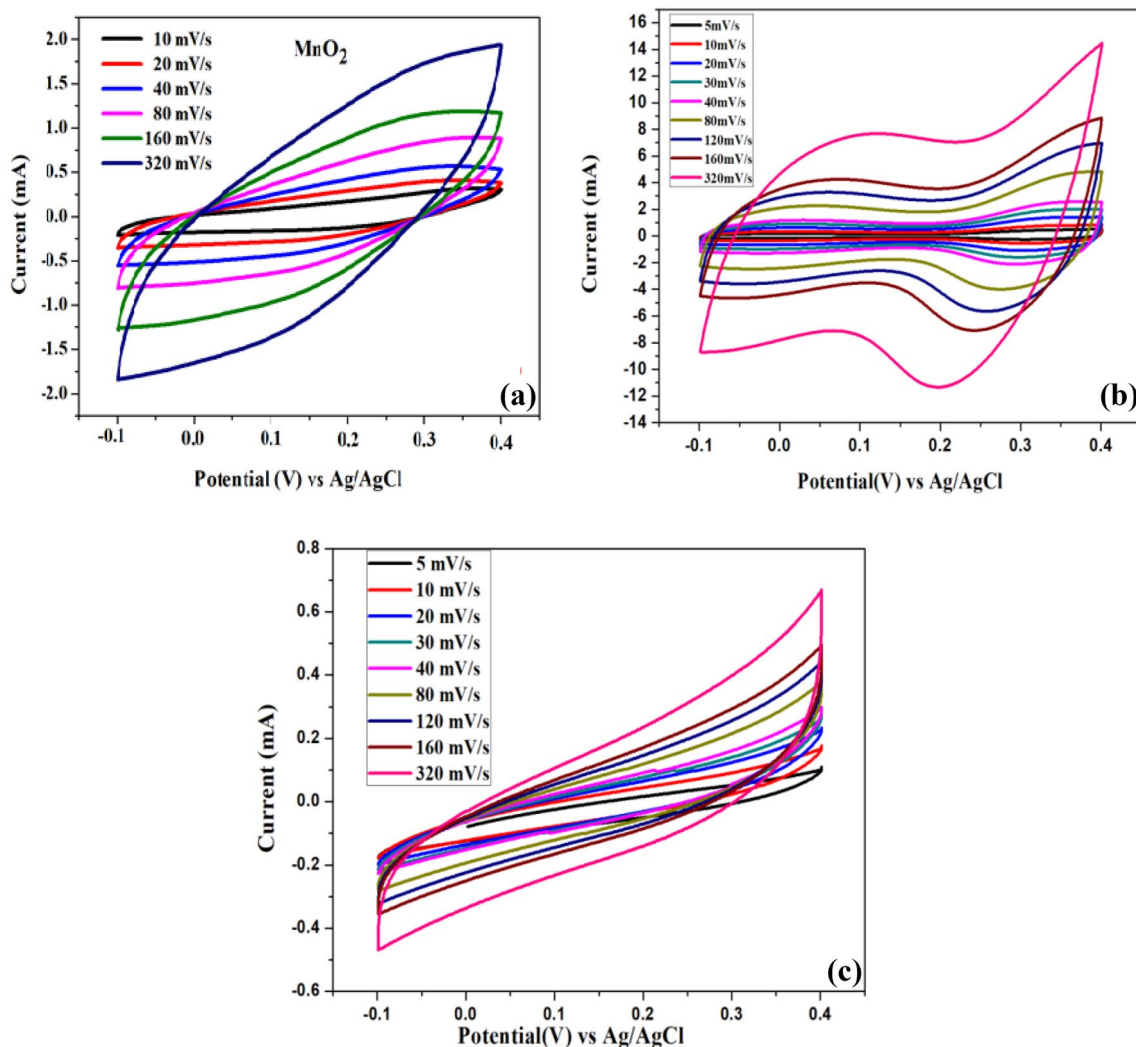


Fig. 7 Cyclic voltammograms at different scan rates of a MnO₂, b NiO and c MnO₂/NiO nanocomposite

prepared in the present work revealed better cycling performance than some of the earlier reports. From the GCD plot, the Coulombic efficiency was calculated by the following equation:

$$\text{Coulombic efficiency} = \left[\frac{\text{discharging time } (t_D)}{\text{charging time } (t_C)} \right] 100\% \tag{4}$$

The Coulombic efficiency (calculated with respect to the second GCD cycle) of MnO₂/NiO is 104%, which is good for potential supercapacitor applications. The GCD test was continued up to 10,000 cycles. To know the cyclic stability of MnO₂/NiO, we have plotted the specific capacitance vs. the number of cycles and it is shown in Fig. 10. After 10,000 cycles, the specific capacitance remains stable and the retention of specific capacitance is 81.2%, which is also excellent for supercapacitor applications.

The kinetics of the above prepared pristine and composite electrodes materials were examined by EIS analysis. The Fig. 11 signifies the MnO₂, NiO and MnO₂/NiO nanocomposite Nyquist plots. EIS of pristine MnO₂, NiO and MnO₂/

NiO nanocomposite were taken in open circuit potential at a frequency sequence of 0.1 Hz to 100 kHz with 10 mV of functional potential amplitude. The Nyquist plot indicates in the high-frequency interval a single semicircle and the low-frequency interval in a linear peak. The arc indicates double-layered capacitance and charge transmission resistance. The occurrence of the point is acknowledged to dispersal of ions neighboring the electrode surface, demonstrating the pseudocapacitive properties of the MnO₂, NiO and

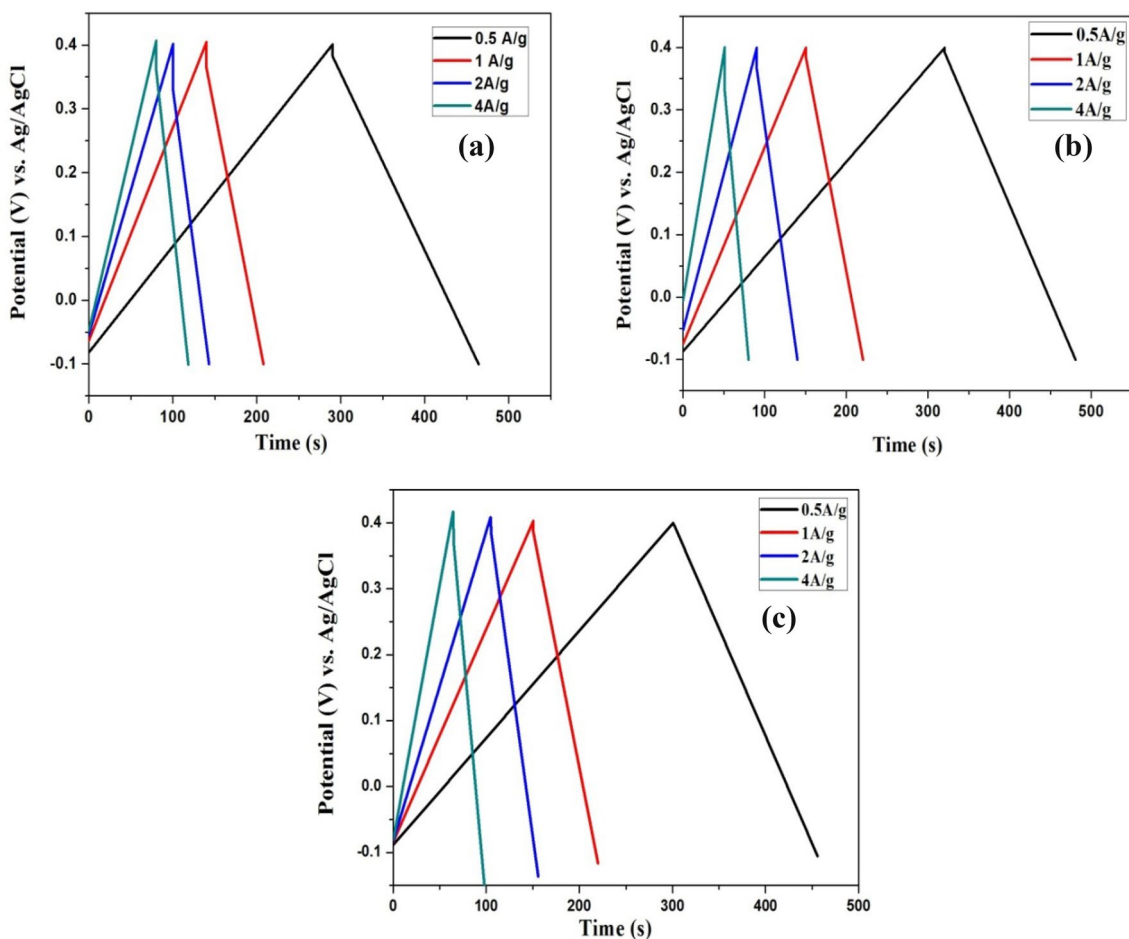


Fig. 8 Charge–discharge curves at different current densities of a MnO₂, b NiO and c MnO₂/NiO nanocomposite

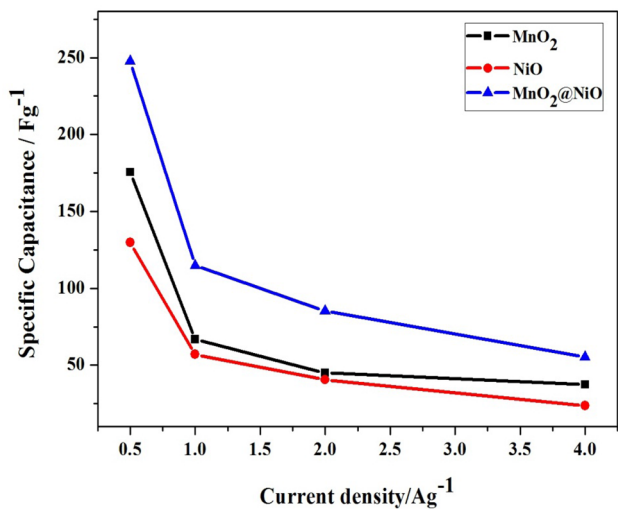


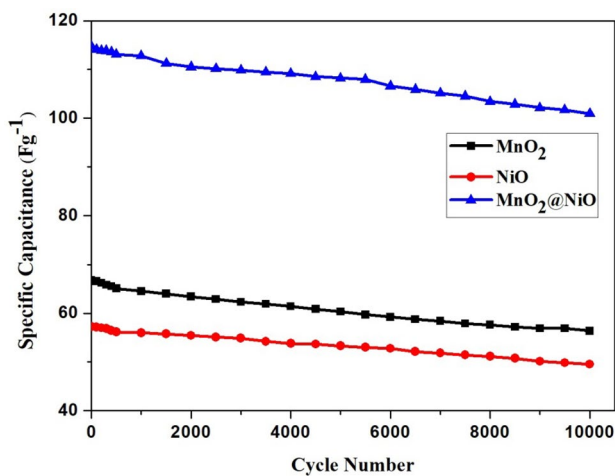
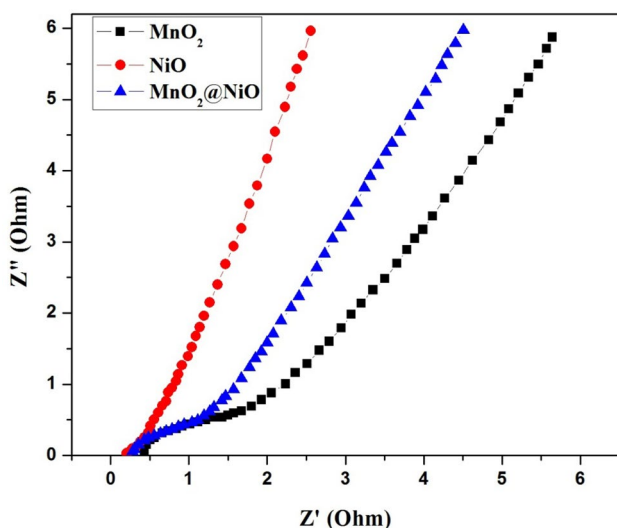
Fig. 9 Specific capacitance (Cs) versus discharge current density of MnO₂, NiO and MnO₂/NiO nanocomposite electrodes

Table 1 Specific capacitance, energy and power density values of MnO₂, NiO and MnO₂/NiO nanocomposite

Sample	Specific capacitance (Fg ⁻¹)	Energy density (Wh kg ⁻¹)	Power density (kW kg ⁻¹)
MnO₂			
0.5 Ag ⁻¹	175.51	6.0904	0.124
1 Ag ⁻¹	66.78	9.2752	0.588
2 Ag ⁻¹	45.15	25.0319	1.999
4 Ag ⁻¹	37.47	83.2695	7.989
NiO			
0.5 Ag ⁻¹	129.65	4.5019	0.101
1 Ag ⁻¹	57.10	7.9182	0.399
2 Ag ⁻¹	40.55	22.5287	1.599
4 Ag ⁻¹	23.72	52.7202	6.398
MnO₂@NiO			
0.5 Ag ⁻¹	247.78	8.6034	0.298
1 Ag ⁻¹	114.76	15.9388	0.797
2 Ag ⁻¹	85.24	47.3582	3.199
4 Ag ⁻¹	56.21	123.1288	12.845

Table 2 Comparison of maximum capacitance values of the reported and the present electrode of MnO₂/NiO composite

Electrode material	Method	Morphology	Electrolyte	Capacitance (F g ⁻¹)	References
MnO ₂ -based mixed oxides	Co-Precipitate	Amorphous	Na ₂ SO ₄ (1 M)	210 Fg ⁻¹ (0.12 Ag ⁻¹)	[38]
Facile synthesis of NiMn ₂ O ₄	Hydrothermal	Nanosheets	Na ₂ SO ₄ (1 M)	370.5 Fg ⁻¹ (1Ag ⁻¹)	[39]
NiO@MnO ₂ core/shell nanocomposites	Hydrothermal	Nanosheets	KOH (2 M)	266.7 Fg ⁻¹ (0.5 Ag ⁻¹)	[27]
α-MnO ₂ /graphene	Solvothermal	Nanorod	Na ₂ SO ₄ (0.5 M)	360 Fg ⁻¹ (2.5 Ag ⁻¹)	[40]
MnO ₂ /graphene hydrogel	Hydrothermal	Honeycomb	KOH (1 M)	278.5 Fg ⁻¹ (1 Ag ⁻¹)	[41]
Ternary NiCo–MnO ₂ nanocomposite	Chemical precipitation	Porous	KOH (1 M)	264.1 (0.5 Ag ⁻¹)	[42]
Binary manganese–nickel oxides	Anodic deposition	Spherical	Na ₂ SO ₄ (0.1 M)	160 Fg ⁻¹	[43]
Nanosized Ni–Mn oxides	Sol–gel technique	Spherical	KOH (4 M)	198.8 Fg ⁻¹	[44]
MnO ₂ @NiO nanocomposites	Hydrothermal	Spherical	KOH (1 M)	247.7 (0.5 Ag ⁻¹)	This Work

**Fig. 10** Cycling performance of the MnO₂, NiO and MnO₂/NiO nanocomposite electrodes**Fig. 11** Nyquist plots of MnO₂, NiO and MnO₂/NiO nanocomposite electrodes

MnO₂/NiO nanocomposite. The semicircle length denotes the charge transfer resistance, ($R_{ct} \approx 2 \Omega$) in the electrochemical technique. The EIS results validate the CV results specifying that the extreme capacitance participation of the composite electrode material is established on the fast surface redox reaction. All of the results indicate that the MnO₂/NiO nanocomposite is a suitable electrode material for supercapacitors.

4 Conclusion

In conclusion, the MnO₂/NiO nanocomposite was successfully prepared by economical hydrothermal method to investigate the electrochemical performance of ultracapacitors. The hydrothermal treatment of metal oxides and their composites at 120 °C produces pure nanostructured oxides after 24 h of reaction. The easy availability, low cost of the reactants and the mild hydrothermal conditions make this method an economic and simple way to produce these materials. The synthesized MnO₂/NiO nanocomposite was characterized using XRD, HRSEM, EDX and TEM. The electrochemical achievements of prepared electrodes have been studied through cyclic voltammetry (CV) and galvanostatic charge/discharge test. The MnO₂/NiO nanocomposite reveals a stable cycle performance and notable rate performance. The structural and surface morphology studies of MnO₂/NiO nanocomposite have revealed nanocrystalline nature. This increased conductivity and uniform morphology of the compound accelerates transfer of electrons and the electrolyte diffusion in the hybrid compounds. The MnO₂/NiO nanocrystalline composite shows a high specific capacity of 247 Fg⁻¹ at a current density of 0.5 Ag⁻¹, energy density of 8.6034 Wh kg⁻¹ and power density of 0.298 kW kg⁻¹ compound with good rate capacity and cyclic stability. Improved electrochemical performance of MnO₂/NiO than pristine MnO₂ and NiO could be considered as potential electrode materials for next generation supercapacitors.

References

- V. Augustyn, P. Simon, B. Dunn, *Energy Environ. Sci.* **7**, 1597–1614 (2014)
- M.R. Lukatskaya, B. Dunn, Y. Gogotsi, *Nat. Commun.* **7**, 12647–12659 (2016)
- Y. Liu, B. Zhang, F. Wang, Z. Wen, Y. Wu, *Pure Appl. Chem.* **86**, 593–609 (2014)
- G.P. Wang, L. Zhang, J.J. Zhang, *Chem. Soc. Rev.* **41**, 797–828 (2012)
- H.B. Wu, G. Zhang, L. Yu, X.W. Lou, *Nanoscale Horiz.* **1**, 27–40 (2016)
- A. Yu, V. Chabot, J. Zhang, *Electrochemical supercapacitors for energy storage and delivery*. CRC Press, Taylor & Francis Group (2013)
- M.S. Nooshabadi, F. Zahedi, *Electrochim. Acta* **245**, 575–586 (2017)
- Z. L. Deng, J. Hao, Wang et al., *Electrochim. Acta* **89**, 191–198 (2013)
- L. Zhao, J. Yu, W. Li, S. Wang, C. Dai, J. Wu, X. Bai, C. Zhi, *Nano Energy* **4**, 39–48 (2014)
- C.-L. Tang, X. Wei, Y.-M. Jiang, X.-Y. Wu, L.N. Han, K.-X. Wang, J.-S. Chen, *J. Phys. Chem. C* **119**, 8465–8471 (2015)
- S.J. Zhu, J.Q. Jia, T. Wang, D. Zhao, J. Yang, F. Dong, Z.G. Shang, Y.X. Zhang, *Chem. Commun.* (2015). <https://doi.org/10.1039/c5cc03976b>
- Y. Hu, J. Wang, *J. Power Sources* **286**, 394–399 (2015)
- W. Li, K. Xu, B. Li, J. Sun, F. Jiang, Z. Yu, R. Zou, Z. Chen, J. Hu, *ChemElectroChem* **1**, 1003–1008 (2014)
- X. Lu, D. Zheng, T. Zhai, Z. Liu, Y. Huang, S. Xie, Y. Tong, *Energy Environ. Sci.* **4**, 2915–2921 (2011)
- K. Xiao, J.-W. Li, G.-F. Chen, Z.-Q. Liu, N. Li, Y.-Z. Su, *Electrochim. Acta* **149**, 341–348 (2014)
- C. Wang, Y. Zhan, L. Wu, Y. Li, J. Liu, *Nanotechnology* **25**, 305401 (2014)
- L.-F. Chen, Z.-H. Huang, H.-W. Liang, Q.-F. Guan, S.-H. Yu, *Adv. Mater.* **25**, 4746–4752 (2013)
- J. Liu, M. Jiang, H.J. Bosman, Fan, *J. Mater. Chem.* **22**, 2419–2426 (2012)
- S.I. Kim, J.S. Lee, H.J. Ahn, H.K. Song, J.H. Jang, *ACS Appl. Mater. Interfaces* **5**, 1596–1603 (2013)
- X. Zhao, L. Zhang, S. Murali, M.D. Stoller, Q. Zhang, Y. Zhu, R.S. Ruoff, *ACS Nano* **6**, 5404–5412 (2012)
- J.P. Liu, J. Jiang, C.W. Cheng, H.X. Li, J.X. Zhang, H. Gong, H.J. Fan, *Adv. Mater.* **23**, 2076–2081 (2011)
- J. Kang, A. Hirata, L. Kang, X. Zhang, Y. Hou, L. Chen, C. Li, T. Fujita, K. Akagi, M. Chen, *Angew. Chem. Int. Ed.* **125**, 1708–1711 (2013)
- C.Z. Yuan, X.G. Zhang, L.H. Su, B. Gao, L.F. Shen, *J. Mater. Chem.* **19**, 5772–5777 (2009)
- Y. Qian, R. Liu, Q.F. Wang, J. Xu, D. Chen, G.Z. Shen, *J. Mater. Chem. A* **2**, 10917–10922 (2014)
- J.P. Liu, J. Jiang, M. Bosman, H.J. Fan, *J. Mater. Chem.* **22**, 2419–2426 (2012)
- Y.H. Li, H.R. Peng, C. Zhang, M.S. Chu, P. Xiao, Y.H. Zhang, *RSC Adv.* **5**, 77115–77121 (2015)
- J. Chen, Y. Huang, C. Li, X. Chen, X. Zhang, *Appl. Surf. Sci.* **360**, 534–539 (2016)
- Y. Bi, A. Nautiyal, H. Zhang, J. Luo, X. Zhang, *Electrochim. Acta* **260**, 952–958 (2018)
- S. Xi, Y. Zhu, Y. Yang, S. Jiang, Z. Tang, *Nanoscale Res. Lett.* **12**, 171 (2017)
- H. Wang, X. Fan, X. Zhang, Y. Huang, Q. Wu, Q. Pan, Q. Li, *RSC Adv.* **7**, 23328 (2017)
- S. Zhu, L. Li, J. Liu, H. Wang, T. Wang, Y. Zhang, L. Zhang, R.S. Ruoff, F. Dong, *ACS Nano* **12**(2), 1033–1042 (2018)
- M. Ma, Y. Zhang, W. Yu, H.Y. Shen, H.Q. Zhang, N. Gu, *Colloids Surf. A* **212**, 219 (2003)
- X. Zhang, Q. Wang, J. Zhang, J. Wang, M. Guo, S. Chen, C. Li, C. Hu, Y. Xie, *RSC Adv.* **5**, 89976–89984 (2015)
- M.M.L. Sonia, S. Anand, V.M. Vinosel, M.A. Janifer, S. Pauline, *J. Mater. Sci. Mater. Electron.* **29**(17), 15006–15021 (2018)
- A.P. Amaliya, S. Anand, S. Pauline, *J. Magn. Magn. Mater.* **467**, 14–28 (2018)
- L.H. Bao, J.F. Zang, X.D. Li, *Nano Lett.* **11**, 1215 (2011)
- J.-H. Kim, K. Zhu, Y.F. Yan, C.L. Perkins, A. Frank, *Nano Lett.* **10**, 4099 (2010)
- H. Kim, B.N. Popov, *J. Electrochem. Soc.* **150**, D56 (2003)
- H. Wei, J. Wang, L. Yu, Y. Zhang, D. Hou, T. Li, *Ceram. Int.* **42**(13), 14963–14969 (2016)
- Y. Haldorai, K. Giribabu, S.K. Hwang, C.H. Kwak, Y.S. Huh, Y.K. Han, *Electrochim. Acta* **222**, 717–727 (2016)
- J. Zhong, F. Yi, A. Gao, D. Shu, Y. Huang, Z. Li, W. Zhu, C. He, T. Meng, S. Zhao, *ChemElectroChem.* **4**, 1088–1094 (2017)
- K.O. Oyedotun, M.J. Madito, D.Y. Momodu, A.A. Mirghni, T.M. Masikhwa, N. Manyala, *Chem. Eng. J.* **335**, 416–433 (2018)
- Y. Chen, C. Hu, *Electrochem. Solid-State Lett.* **6**, 210–213 (2003)
- J. Zhou, X. Shen, M. Jing, *J. Mater. Sci. Technol.* **22**, 803–806 (2006)

Publisher's Note Springer Nature remains neutral with regard to jurisdictional claims in published maps and institutional affiliations.